

Models for diffusion and island growth in metal monolayers

Ofer Biham* and Itay Furman

Racah Institute of Physics, The Hebrew University, Jerusalem 91904, Israel

Majid Karimi

Physics Department, Indiana University of Pennsylvania, Indiana, PA 15705

Gianfranco Vidali, Rosemary Kennett and Hong Zeng

Department of Physics, Syracuse University, Syracuse, NY 13244

A model that describes self diffusion, island nucleation and film growth on FCC(001) metal substrates is presented. The parameters of the model are optimized to describe Cu diffusion on Cu(001), by comparing activation energy barriers to a full set of barriers obtained from semi-empirical potentials via the embedded atom method. It is found that this model (model I), with only three parameters, provides a very good description of the full landscape of hopping energy barriers. These energy barriers are grouped in four main peaks. A reduced model (model II) with only two parameters, is also presented, in which each peak is collapsed into a single energy value. From the results of our simulations, we find that this model still maintains the essential features of diffusion and growth on this model surface. We find that hopping rates along island edges are much higher than for isolated atoms (giving rise to compact island shapes) and that vacancy mobility is higher than adatom mobility. We observe substantial dimer mobility (comparable to the single atom mobility) as well as some mobility of trimers. Mobility of small islands affects the scaling of island density N vs. deposition rate F , $N \sim F^\gamma$, as well as the island size distribution. In the asymptotic limit of slow deposition, scaling arguments and rate equations show that $\gamma = i^*/(2i^* + 1)$ where i^* is the size of the largest mobile island. Our Monte Carlo results, obtained for a range of experimentally relevant conditions, show $\gamma = 0.32 \pm 0.01$ for the EAM, 0.33 ± 0.01 for model I and 0.31 ± 0.01 for model II barriers. These results are lower than the anticipated $\gamma \geq 0.4$ due to dimer (and trimer) mobility.

arXiv:cond-mat/9611095v2 [cond-mat.mtrl-sci] 15 Feb 1998

*Tel:972-2-6584363;Fax:972-2-6520089;Email:biham@flounder.fiz.huji.ac.il

I. INTRODUCTION

Recent experiments on thin film growth on well characterized substrates using molecular beam epitaxy have provided detailed information about growth kinetics and morphology. In particular, growth in the submonolayer regime has been studied extensively using both scanning tunneling microscopy (STM) [1–10] and diffraction methods such as helium atom beam scattering [11–13] and low energy electron diffraction [14–16]. It was observed that for a variety of systems and a broad temperature range, island nucleation is the dominant mechanism for crystal growth. A variety of island morphologies has been found. Fractal-like islands, resembling diffusion limited aggregation (DLA) clusters, were observed in Au on Ru(0001) [2,3], Cu on Ru(0001) [3] and Pt on Pt(111) [4,5]. On the other hand, compact islands were observed in Ni on Ni(001) system [6]. Scaling properties of the island density as a function of deposition rate and coverage, as well as the island size distribution have been studied experimentally by several groups [7,8,10,11,14,15]. Field ion microscopy (FIM) experiments that provide direct access to diffusion processes at the atomic scale, have also been performed [17–19]. This technique was used to identify the diffusion modes of adatoms [17] as well as small islands [18,19] on FCC(001) metal surfaces and to measure their diffusion coefficients.

Theoretical studies aimed at providing a better understanding of the relation between key processes at the atomic scale and the resulting morphologies have been done using Monte Carlo (MC) simulations [20–35]. In simulations of island growth during deposition, atoms are deposited randomly on the substrate at rate F [given in monolayer (ML) per second] and then hop according to a microscopic model. The hopping rate h (in units of hops per second) of a given atom to each unoccupied nearest neighbor (NN) site is given by

$$h = \nu \cdot \exp(-E_B/k_B T) \quad (1)$$

where $\nu = 10^{12} \text{ s}^{-1}$ is the commonly used attempt rate, E_B is the activation energy barrier, k_B is the Boltzmann constant and T is the temperature.

The activation energy barrier E_B depends on the local environment of the hopping atom, namely the configuration of occupied and unoccupied adjacent sites. Two approaches have been taken in the construction of the energy barriers for hopping. One approach was to construct simple models that include the desired features, such as stability and mobility of small islands, and that take into account properties such as bond energies [20–23,25,26,28–31,33–35]. The advantage of this approach is that the models are well defined and use only a few parameters. These models are useful for studies of scaling and morphology but cannot provide a quantitative description of diffusion on a particular substrate. A second approach is based on the use of an approximate many-body energy functional to calculate the hopping

energy barriers for a complete set of relevant configurations [24,27,32]. This approach provides a good description of diffusion processes on the given substrate but only limited understanding due to the large number of parameters.

In this work we propose a procedure that combines the advantages of both approaches. Using sensible assumptions about the bond energies and diffusion paths we obtain a simple formula for the activation energy barriers. We then optimize the parameters of this formula by using energy barriers obtained from the embedded atom method for Cu diffusion on Cu(001). This procedure provides two simple models which combine the best features of both approaches. Model I, which has three parameters, provides good quantitative description of the landscape of hopping energy barriers. Model II, which has only two parameters and is as simple as other minimal models, still incorporates the essential physics of diffusion of adatoms on FCC(001) metal surfaces.

We find that on the Cu(001) substrate, edge mobility (i.e., the mobility of an adatom at the perimeter of an island) is much higher than the single adatom mobility, giving rise to compact island shapes. Dimer mobility is comparable to the single adatom mobility while trimers are also mobile [27,36,37]. Mobility of small islands has a significant effect on the asymptotic scaling properties and is thus particularly important. We also find that vacancies have higher mobility than adatoms.

The paper is organized as follows. In Section II we introduce the models. Simulation and results are presented in Section III with emphasis on scaling and morphology. The results and their implications are discussed in Section IV and a summary is given in Section V.

II. THE MODELS

A. The EAM Barriers

In this work we use a set of energy barriers for Cu on Cu(001) [38] obtained using the embedded atom method (EAM) [39]. This method uses semiempirical potentials and provides a good description of self diffusion of Cu on Cu(001) and similar surfaces [38]. Specifically, we use the EAM functions of Cu developed by Adams, Foiles, and Wolfer [40] which are fitted to a similar data base as the one employed by Foiles, Baskes, and Daw [41].

The hopping energy barriers are calculated for all local environments as shown in Fig. 1, where seven adjacent sites, $i = 0, \dots, 6$ are taken into account [42]. Each one of these sites can be either occupied ($S_i = 1$) or vacant ($S_i = 0$), giving rise to $2^7 = 128$ barriers. A binary representation is used to assign indices to these barriers. For each configuration (S_0, \dots, S_6) the barrier is given by E_B^n , where

$$n = \sum_{i=0}^6 S_i \cdot 2^i \quad (2)$$

takes the values $n = 0, \dots, 127$. The full set of hopping energy barriers (given in eV) is presented in Table I. To show these values in a compact form, each barrier in Table I corresponds to a configuration in which the occupied sites are the union of the occupied sites in the picture on top of the given column and on the left hand side of the given row. The column in Table I in which a given configuration appears is determined by the occupancy of sites $i = 2, 3, 6$ while the row is determined by sites $i = 0, 1, 4, 5$. One can define

$$n_1 = \sum_{i=2,3,6} S_i \cdot 2^i; \quad n_2 = \sum_{i=0,1,4,5} S_i \cdot 2^i \quad (3)$$

such that for each configuration $n = n_1 + n_2$. To demonstrate the use of Table I, we will check the barrier for the configuration in which sites 0, 3 and 4 are occupied and all other sites adjacent to the hopping atom are vacant. For this configuration, according to Eq. (3), $n_1 = 8$ and $n_2 = 17$ ($n = 25$). The barrier, which is found in the column with the index 8 and the row with index 17, is $E_B^{25} = 0.89$ eV.

In Table I we use the symmetries of the configurations in the 3×3 cell to reduce the number of entries. There is a mirror symmetry plane perpendicular to the surface and containing the arrow of the hopping atom. Consequently, the columns of $n_1 = 4$ and 12, in which site $i = 2$ is occupied, stand also for the symmetric configurations in which $i = 6$ is occupied. In the other four columns, there are some configurations that, due to symmetry, appear twice. In such cases, the barrier for the configuration with larger n appears in *italics*.

Here we consider only hopping moves in which a single atom hops each time. However, it turns out that in some cases the molecular statics calculations, used to obtain the barriers, give rise to concerted moves. In such moves the atom at site $i = 3$ follows the hopping atom and takes the place vacated by the hopping atom. This fact significantly reduces the barrier. We have found that for all configurations in which concerted moves appear, these concerted moves can be suppressed by adding one more row of atoms on the left hand sides of sites $i = 0, 3$ and 4. In Table I, the energy values for those configuration in which a concerted move was found, are shown in parenthesis. The barrier obtained when the concerted move was suppressed is shown to the left of the parenthesis.

Concerted moves may affect film growth by modifying either the stability and mobility of small islands or the morphology of large islands. The effect of the shear move ($n_1 = 8$; $n_2 = 3$), in which concerted motion reduces the barrier from $E_B^{11} = 0.78$ eV to 0.65 eV, was studied in Ref. [43]. It was claimed that for experiments with very low deposition rates this move effectively raises i^* from 3 to 8, where i^* is the size of the critical island nucleus. Simple calculations of the hopping rates, using

Eq. (1) indicate that, since the reduced barrier is still rather large, the effect of this concerted move is negligible for the temperatures and deposition rates studied in this paper.

We find that there are other concerted moves which, unlike the shear move discussed above, cause a dramatic reduction in the barrier for the given move (Table I). If the atoms inside the 3×3 square represent an isolated island and sites around are vacant, it is easy to see that moves such as $(n_1, n_2) = (34, 12)$, and $(35, 76)$ simply lead to a more stable configuration of the pentamer and heptamer islands, respectively. Once this more stable configuration is obtained, the concerted move cannot take place again. Since these more stable configurations can be obtained through other fast moves, the concerted move does not have a significant effect on the overall morphology of the film. Other moves such as $(34, 8)$, $(50, 12)$, and $(51, 76)$ can occur only as long as the islands of 4, 6 and 8 atoms respectively, have not reached their most stable configuration. If the above configurations, in which concerted moves are possible, occur in a denser environment, and in particular if the sites on the left hand side of sites $i = 0, 3$ and 4 are occupied, the concerted moves are suppressed. Thus, we conclude that in both cases the concerted moves do not have a significant effect in the simulations presented here and they will be ignored.

To gain a better understanding of the barrier energy landscape we discuss the barrier height distribution (without concerted moves) in Fig. 2(a). We observe that this distribution exhibits four peaks. This feature is in agreement with Ref. [44] where a different method [45] was used to calculate the barriers. Each peak, corresponds to a single or a double column in Table I (there is a little ambiguity in the region between peaks III and IV due to a slight overlap). In general, peak I includes very fast moves toward island edges, peak II includes moves along the edge, peak III includes, most notably, the single atom move, while peak IV includes detachment moves.

B. Construction of Models

When an atom on the surface hops into a vacant nearest neighbor site it has to cross the energy barrier between the initial and final sites. We have used molecular statics in conjunction with EAM functions to find the diffusion path of an adatom. Not surprisingly, we have found that the top of the energy barrier to go from a four-fold coordinate site to an adjacent site is at the bridge site. By slowly moving the adatom within the molecular statics calculation, it turns out that the hopping energy barrier is simply the difference between the energy at the bridge site and in the initial site. The occupancy of the seven adjacent sites (Fig. 1) affects both energies. We will now express the energy of the hopping atom in its initial site as:

$$E_{in} = E_{in}^0 - \Delta E_{in} \cdot (S_1 + S_3 + S_5) - \Delta E_{in}^{nnn} \cdot (S_0 + S_2 + S_4 + S_6) \quad (4)$$

where $S_i = 1$ if site i is occupied and 0 otherwise. The energy of an isolated atom is E_{in}^0 while the reduction in its energy due the presence of an atom in a nearest (next nearest) neighbor site is given by ΔE_{in} (ΔE_{in}^{nnn}). Here we assume that the contributions of nearest neighbor and next nearest neighbor (NNN) atoms to the energy are additive. The energy of the hopping atom when it is on the bridge site is given by:

$$E_{top} = E_{top}^0 - \Delta E_{top} \cdot (S_1 + S_2 + S_5 + S_6) \quad (5)$$

where E_{top}^0 is the energy of an isolated atom on top of a bridge site, while ΔE_{top} is the reduction in the energy due to the presence of an atom in one of the four sites adjacent to the bridge site. We do not include here NNN type contributions since their effect is small. Therefore, for a given configuration the barrier $E_B = E_{top} - E_{in}$ for an atom to hop into an adjacent vacant site is given by:

$$E_B^n = E_B^0 - \Delta E_{top} \cdot (S_2 + S_6) + \Delta E_{in} \cdot S_3 - (\Delta E_{top} - \Delta E_{in}) \cdot (S_1 + S_5) + \Delta E_{in}^{nnn} \cdot (S_0 + S_2 + S_4 + S_6) \quad (6)$$

where $E_B^0 = E_{top}^0 - E_{in}^0$ and n is given by Eq. (2). To examine the formula above, we found the parameters that best describe the 128 EAM barriers by minimizing the sum of squares

$$R = \sum_{n=0}^{127} [E_B^n(\text{EAM}) - E_B^n(\text{Eq. 6})]^2. \quad (7)$$

The values obtained for the parameters in Eq. (6) are $E_B^0 = 0.494$, $\Delta E_{in} = 0.265$, $\Delta E_{top} = 0.268$ and $\Delta E_{in}^{nnn} = 0.024$ eV. Thus, we find that to within about 0.003 eV, $\Delta E_{in} = \Delta E_{top}$. Replacing both ΔE_{in} and ΔE_{top} by $\Delta E = 0.265$ eV we obtain a three parameter model (model I) in which the energy barriers are:

$$E_B^n = E_B^0 + \Delta E \cdot (S_3 - S_2 - S_6) + \Delta E_{in}^{nnn} \cdot (S_0 + S_2 + S_4 + S_6) \quad (8)$$

where n is given by Eq. (2). The distribution of energy barriers obtained from Eq. (8) is shown in Fig. 2(b). A very good agreement in the location of the four peaks with the EAM energy barriers is found, but EAM peaks are significantly broader. This can be due to the fact that during the hopping move adjacent atoms can relax within their potential well. Model I accounts for these effects only on average and therefore gives rise to narrower peaks.

One can further simplify the model by ignoring the NNN interactions which are relatively small, namely choosing $\Delta E_{in}^{nnn} = 0$. This model (model II) has only two parameters and is described by:

$$E_B^n = E_B^0 + \Delta E \cdot (S_3 - S_2 - S_6) \quad (9)$$

where n is given by Eq. (2). Repeating the optimization procedure of Eq. (7) for the barriers given by Eq. (9), we obtain $E_B^0 = 0.526$ and $\Delta E = 0.255$. In this model, all the energy barriers in each peak collapse into a single value. In spite of its simplicity, this model provides a good description of self diffusion of Cu on the Cu(001) substrate.

C. Diffusion Coefficients

To find out which island sizes are mobile and to obtain the diffusion coefficients of mobile islands on Cu(001), we have done simulations of single cluster diffusion. To obtain the statistics required for a precise determination of the diffusion coefficients we performed 1000 runs for diffusion of monomers, dimers, trimers, pentamers ($s = 5$) and heptamers ($s = 7$). Each run was carried out for a time equal to 1.0 seconds, which is more than 100 times larger than the time scale for hopping of an isolated adatom at the given temperature ($T = 250\text{K}$). The diffusion coefficients were obtained from the relation $\langle r^2 \rangle = 4h_s t$, where $s = 1, 2, 3, 5, 7$ is the number of atoms in the cluster, r is the distance between the initial position of the center of mass of the cluster and its position after time t , h_s is the diffusion coefficient for a cluster of size s and $\langle \dots \rangle$ represents an average over the 1000 runs. The diffusion coefficients for monomers, dimers, trimers, pentamers and heptamers are shown in Table II. It is also found that under the conditions studied here the diffusion coefficients for islands of size $s = 4, 6$ and $s \geq 8$ are negligible.

III. SIMULATIONS AND RESULTS

A. Monte Carlo Simulations

To assess the validity of our models, we have performed MC simulations of island growth for a range of deposition rates using the EAM as well as model I and model II barriers [46]. We used a continuous time MC technique [47–50,27] in which moves are selected randomly from the list of all possible moves at the given time with the appropriate weights. The time is advanced after each move according to the inverse of the sum of all rates. The existence of four peaks in the spectrum of energy barriers indicates that there are four typical time scales of hopping. The two lowest peaks include very fast moves towards and along island edges and motion of vacancies. The single atom move is in the third peak while moves in which atoms detach from islands are in the highest peak.

From statistics collected during the simulations we find that most of the computer time is consumed by moves $n = 6$ (96) and 7 (112). The first move occurs in trimers

while both moves occur for atoms hopping along straight island edges. The reason that these moves consume so much time is that the reverse move typically has the same low barrier so the atom can continuously hop back and forth for a long time. To make the simulation feasible, we had to somewhat suppress these moves by artificially raising the barriers in the first and second peaks. This was done for all barriers lower than 0.4 eV according to: $E_B^n \rightarrow E_B^n + \alpha(0.4 - E_B^n)$ where $\alpha = 0.7$. Since the moves associated with these barriers are still orders of magnitude faster than for the two higher peaks we expect that this modification will have only small effect on the island morphology. We tried various values of α and found that up to $\alpha \approx 0.8$ this is indeed the case.

B. Island Growth and Morphology

In Fig. 3 we show the island morphologies obtained in MC simulations using the energy barriers from EAM [Fig. 3(a)], model I [Fig. 3(b)] and model II [Fig. 3(c)]. These simulations were done on a 250×250 lattice at $T = 250\text{K}$ and deposition rate $F = 0.01$ ML/s. The snapshots presented here are for a coverage $\theta = 0.1$ ML. These snapshots indicate that models I and II provide a good description of the model with the full EAM barriers as far as the island morphology is concerned. The islands are rather compact, dominated by overall square and rectangular shapes with a small number of kinks.

The island density vs. coverage is presented in Fig. 4 for the EAM (*), model I (o) and model II (+) energy barriers. In all cases the island density quickly increases at low coverage, then saturates and remains nearly constant thereafter. It starts to decrease at higher coverage, when coalescence sets in. For model I the island density is slightly higher than for the EAM barriers while for model II it is about 60% higher. These differences are not intrinsic to the models. They can be traced to the fact that the single atom hopping energy barriers obtained from the optimization procedure that we use are $E_B^0 = 0.494$ eV for model I and $E_B^0 = 0.526$ eV for model II; these values are higher than the value of $E_B^0 = 0.485$ eV from the EAM calculations. These discrepancies could be fixed by an overall rescaling of the barriers in each model so that the single atom barrier would be exactly equal to the EAM value. Since there is some arbitrariness in this procedure we chose not to apply it in the simulations presented here. The important result of this work is that our models reproduce the essential features of diffusion, island growth and scaling. The overall factor in island density to make the models agree with the EAM calculations could be obtained by rescaling. While model I reproduces the spectrum of EAM energy barriers more accurately, the importance of model II is that it captures the essential features of adatom diffusion on the Cu(001) in spite of its simplicity.

Snapshots of the island morphology using the EAM

barriers for three deposition rates, $F = 0.1, 0.01$ and 0.001 ML/s are presented in Fig. 5(a)-(c), respectively. The simulations were done on a 250×250 lattice at $T = 250\text{K}$ and the snapshots were taken at $\theta = 0.1$ ML. It is observed that decreasing the deposition rate gives rise to fewer and larger islands. In Fig. 6 we present the island density vs. coverage for the EAM barriers, at deposition rates (from top to bottom) $F = 0.1, 0.04, 0.01, 0.004, 0.001$ and 0.0004 ML/s. It is observed that in addition to the decrease in island density as the deposition rate decreases, the plateau becomes broader and flatter.

C. Scaling Properties

The island density vs. deposition rate is presented in Fig. 7 for the EAM (*), model I (o) and model II (+) energy barriers for $T = 250\text{K}$ and $\theta = 0.1$ ML. This coverage is well within the quasi-steady state regime in which the island density is nearly constant (see Fig. 6). In this regime scaling arguments and rate equations indicate that in the asymptotic limit of low deposition rate the island density exhibits power law behavior of the form

$$N \sim \left(\frac{F}{4h_1} \right)^\gamma \quad (10)$$

where h_1 is the adatom diffusion coefficient (the hopping rate for an isolated atom is $4h_1$ due to the four possible directions for hopping). The exponent γ depends on microscopic properties of the system such as stability [51–53,30,34,54] and mobility [55,35] of small islands, anisotropic diffusion [1,10] and magic islands (islands which are stable while larger islands are unstable) [29]. It was found that for systems in which the smallest stable island is of size $i^* + 1$ (where islands of size $s \leq i^*$ dissociate), $\gamma = i^*/(i^* + 2)$. In this case i^* is the critical island size [51].

Under the conditions studied here, detachment of atoms from islands is negligible, while mobility of small islands is a significant effect. Therefore, we define here the critical island size i^* as the size for which all islands of size $s \leq i^*$ are mobile while islands of size $s \geq i^* + 1$ are immobile. In this case the asymptotic value of γ in the limit where $F/h_1 \rightarrow 0$ is given by [55,35]:

$$\gamma = \frac{i^*}{2i^* + 1}. \quad (11)$$

This result is exact if all mobile islands have the same diffusion coefficient, namely $h_s = h$, $s = 1, \dots, i^*$. Still, it is a good approximation if all the diffusion coefficients are of the same order of magnitude. Table II shows that the diffusion coefficients of pentamers and heptamers are practically negligible. For EAM the diffusion coefficient of the trimer is also rather small and we expect the system to be described by $i^* = 2$. Models I and II exhibit

small but not negligible mobility of trimers and therefore we expect them to be described by either $i^* = 2$ or $i^* = 3$.

In Fig. 7 we observe nearly two and a half decades of scaling behavior, in a range of deposition rates between $F = 0.1$ and 0.0004 ML/s. The best fit through the six data points provides $\gamma = 0.32 \pm 0.01$ for the EAM, 0.33 ± 0.01 for model I and 0.31 ± 0.01 for model II barriers. These results are significantly lower than the asymptotic values for $i^* = 2$ ($\gamma = 2/5$) or $i^* = 3$ ($\gamma = 3/7$). In Ref. [35] a similar deviation was found between simulation results and the asymptotic predictions of the rate equations. It was argued that this deviation is due to the slow convergence of γ to its asymptotic value, when the deposition rate F is lowered. This conclusion is strengthened by the fact that if only the four left-most data points are used in the linear fit, the resulting γ equals 0.35 ± 0.01 for the EAM, 0.36 ± 0.01 for model I and 0.34 ± 0.01 for model II. These results are somewhat closer to the asymptotic value. Moreover, within the error bars they are larger than the asymptotic value that arises from adatom mobility alone, namely $\gamma = 1/3$. Therefore, the possibility that γ converges to $1/3$ should be discarded. Since the conditions used here are experimentally relevant, our results indicate that one should be careful in drawing conclusions about processes at the atomic scale from scaling results (see Section IV D).

The scaling properties of the island size distribution have been studied both experimentally [14,7] and theoretically [22,23,29,30,34,35]. These studies indicated that the island size distribution depends on the stability and mobility of small islands and is modified in the case of magic island sizes [29]. The scaled island size distributions are presented for the three models in Fig. 8. For all three models the deposition rates are $F = 10^{-1}$ (*), 10^{-2} (o) and 10^{-3} ML/s (+). These results are based on statistics collected from 20 runs on a 250×250 size lattice at $T = 250\text{K}$ and $\theta = 0.1$ ML.

The general shape of the distributions seems to resemble previous results [35] for $i^* = 2, 3$ where the peaks rise more slowly on the left hand size (small s/\bar{s}) due to the depletion of the mobile islands. This trend is qualitatively similar to the results for the case where small islands are unstable, as shown in Ref. [30,34]. Note also that the peak height increases considerably as F decreases. This may be due to coalescence which is found to become more pronounced as the deposition rate decreases. Coalescence causes \bar{s} to increase, pushing up the scaled island size distribution which includes the factor \bar{s}^2/θ .

IV. DISCUSSION

A. Small-Island Mobility

For both the EAM barriers and models I and II we obtain significant dimer mobility. The trimer mobility for the EAM barriers is rather small, and somewhat larger in models I and II. In general, we find that the energy barriers relevant for dimer and trimer mobility are in the same peak as the single atom hopping. The differences in hopping rates between monomers, dimers and trimers are due to very small differences in the energy barriers, which at $T = 250\text{K}$ are significant. These differences in hopping rates decrease as the temperature increases. In model II, which has only one activation barrier for each peak, the activation barriers for monomer, dimer and trimer mobilities are all equal. Combinatorial summation of paths then shows that for model II the diffusion coefficient of dimers (trimers) is equal to one half (one quarter) of the monomer diffusion coefficient, at all temperatures. Therefore, in model II, at any temperature in which atoms are mobile, dimers and trimers are also mobile. The mobility of small islands has a significant effect on the asymptotic scaling of the island density vs. deposition rate. In principle, this can be used to extract these diffusion properties at the atomic scale from STM and diffraction results at larger scales. However, our simulations indicate that for experimentally relevant parameters the system is likely to be away from the asymptotic regime, and therefore one should be careful in drawing conclusions from the empirically determined scaling exponents. The relation between mobility of small islands and edge mobility was examined in Ref. [35]. It was shown that both types of mobilities are generated by the same hopping moves and are therefore related, namely, small island mobility implies edge mobility.

B. Edge Mobility

We have found that for Cu(001) atom mobility along straight island edges (for which the barriers belong to peak II) is much higher than the single atom mobility (with a barrier in peak III). This indicates, using an argument from Ref. [28], that islands should form compact shapes for a broad range of temperatures. This conclusion is confirmed by our MC simulations and is in agreement with STM results [6]. For the temperature studied here detachment of atoms from islands is negligible and therefore edge mobility is the dominant process which shapes the islands.

C. Vacancy Mobility

It is found that for Cu(001) the mobility of a single vacancy is higher than the single adatom mobility. We observe that the barrier for the diffusion of a single vacancy is sensitive to the environment beyond the 3×3 square

used to calculate energies in this paper. The energy barrier for diffusion of a single vacancy is $E_B^{127} = 0.12$ eV if all sites around the 3×3 square are vacant. Adding three more atoms on the left it increases it to 0.28 eV. Embedding the hopping vacancy in an occupied 5×5 square increases the barrier to 0.31 eV while the barrier for a single vacancy in the substrate is found to be 0.43 eV (using a slab of 20 layers, 121 atoms/layer). We conclude that, although the vacancy mobility is higher than the adatom mobility, at high coverage the difference may not be dramatic [37]. For example, at low temperature a difference of 0.05 eV in the barrier may significantly affect the hopping rate. A more general conclusion is that models I and II best describe diffusion and nucleation at relatively low coverage. At high coverage, far beyond the percolation threshold hopping can be considered primarily as motion of vacancies. When the adlayer is already dense, relaxation effects during the moves are more important than at low coverage, and the configuration of occupied sites beyond the 3×3 square used here may affect the energy barriers. In spite of the prediction that a single vacancy is more mobile than an adatom, note that for Ag(001) there is evidence that vacancy clusters have lower diffusivity than islands [56].

D. Comparison with Experiments

The simulations presented here were carried out with parameters typical to homoepitaxial growth experiments on Cu(001) surfaces, namely, linear lattice size of 250 sites (about 650 Å), $T = 250$ K and F between 4×10^{-4} and 10^{-1} ML/s [11,15]. In Ref. [15]. $\gamma = 0.33$ was measured for $T = 223$ K, F between 2.5×10^{-4} and 10^{-3} ML/s, and coverage $\theta = 0.3$. This value of γ is in a very good agreement with our simulation results. The authors of Ref. [15] claimed that this indicates that in this system and parameter range, $i^* = 1$. Our results indicate that in this parameter range the system is away from the asymptotic regime. Thus, the value $\gamma = 0.33$ can be obtained even though $i^* = 2$ or 3. A value of $\gamma = 0.55$ was reported (for $T = 223$ K, and F between 10^{-3} and 5×10^{-3}) and $\gamma = 0.58$ (for $T = 263$ K, and F between 2.5×10^{-4} and 10^{-3}) in the same coverage, $\theta = 0.3$ [15]. These values are close to those reported in Ref. [11], namely $\gamma = 0.54$ (for $T = 220$ K, and F between 6.7×10^{-4} and 3.3×10^{-3}), and $\gamma = 0.46$ (for $T = 230$ K, and F between 4×10^{-4} and 10^{-2}). A possible interpretation of the higher values of γ observed in these experiments, is that processes such as coalescence become significant as the coverage increases.

E. Diffusion on Other FCC(001) Metal Surfaces

We expect our approach to apply also to other FCC(001) metal surfaces such as Ni(001) and Ag(001) in which diffusion occurs through hopping rather than by

the exchange mechanism. EAM calculations for Ni(001) and Ag(001) are consistent with our models [57]. For surfaces in which the exchange mechanism is favorable, as it is believed to be the case for Al [58], Pt [17], Pd and Au [59] modifications of the models are required. However, we believe that the approach presented here should still provide a simple and useful model for diffusion on these surfaces.

V. SUMMARY

We have studied adatom self diffusion and island growth on Cu(001) using MC simulations at the atomic scale. As input to the MC simulation we used a complete set of energy barriers obtained from the embedded atom method. To reduce the number of parameters and to obtain better understanding of the diffusion processes we have constructed two simple models. Model I, with three parameters, provides a good quantitative description of the full landscape of hopping energy barriers. Model II, with only two parameters, is a minimal model which still incorporates the essential features of adatom diffusion on the Cu(001) surface.

We examined the diffusion properties of small islands and found that the mobility of dimers is comparable to the single adatom mobility while trimers are also somewhat mobile. The mobility of adatoms along island edges was found to be much higher than the single adatom mobility. Since atoms detachment from islands is negligible, edge mobility is the dominant process that shapes islands into the compact forms. A further conclusion from the EAM calculations is that vacancy mobility, which is dominant at very high coverages, is higher than the single adatom mobility, which is dominant at low and intermediate coverages.

MC simulations of island growth show similar morphologies for the EAM barriers and models I and II. In all cases the islands generally form square or rectangular shapes with a small number of kinks. Studies of the scaling of the island density N vs. deposition rate F show that $N \sim F^\gamma$ where $\gamma = 0.32 \pm 0.01$ for the EAM, 0.33 ± 0.01 for model I and 0.31 ± 0.01 for model II barriers. These results are lower than the asymptotic value of $\gamma \geq 0.4$ anticipated for systems that exhibit dimer (and even trimer) mobility. It indicates that for the experimentally relevant conditions studied here the system has not reached the asymptotic regime. This result call for caution in using scaling results to draw conclusions about diffusion properties at the atomic scale.

Since both models I and II have only few parameters, one needs a very small set of calculated energy barriers to determine these parameters for a given FCC(001) substrate, and a few more barriers to verify that the model applies to that substrate. This may open the way for a more effective use of first principle calculations of energy barriers on the surface as an input to the kinetics calcu-

lations. We believe that the procedure described in this paper would prove useful much beyond the FCC(001) metal substrates. We expect it to be applicable with some modifications to take into account exchange moves which are believed to be favorable in Al,Pt,Pd and Au. We believe that the approach presented here will provide useful models for adatom self diffusion on FCC(111) surfaces, for which reliable calculations of energy barriers are becoming available [60,61], and also to a variety of heteroepitaxial systems.

ACKNOWLEDGMENTS

OB would like to thank Oded Millo and Nira Shimon for helpful discussions. We would like to acknowledge partial support from the NSF under grants DMR-9217284 and DMR-9119735 at Syracuse University during the initial stages of this work and partial support from Intel-Israel college relations committee during the final stages.

-
- [1] Y. W. Mo, J. Kleiner, M. B. Webb and M. G. Lagally, *Phys. Rev. Lett.* **66** (1991) 1998.
- [2] R. Q. Hwang, J. Schroder, C. Gunther and R. J. Behm *Phys. Rev. Lett.* **67** (1991) 3279.
- [3] G. Potschke, J. Schroder, C. Gunther, R.Q. Hwang and R.J. Behm, *Surf. Sci.* **251** (1991) 592.
- [4] M. Bott, T. Michely and G. Comsa, *Surf. Sci.* **272** (1992) 161.
- [5] T. Michely, M. Hohage, M. Bott and G. Comsa, *Phys. Rev. Lett.* **70** (1993) 3943.
- [6] E. Kopatzki, S. Gunther, W. Nichtl-Pecher and R. J. Behm *Surf. Sci.* **284** (1993) 154.
- [7] J. A. Strosio and D. T. Pierce, *Phys. Rev.* **B49** (1994) 8522.
- [8] S. Gunther, E. Kopatzki, M.C. Bartelt, J.W. Evans and R.J. Behm *Phys. Rev. Lett.* **73** (1994) 553.
- [9] S. Esch, M. Hohage, T. Michely and G. Comsa, *Phys. Rev. Lett.* **72** (1994) 518.
- [10] T.R. Linderoth, J.J. Mortensen, K.W. Jacobsen, E. Laegsgaard, I Stensgaard and F. Besenbacher, *Phys. Rev. Lett.* **77** (1996) 518.
- [11] H.-J. Ernst, F. Fabre and J. Lapujoulade, *Phys. Rev.* **B46** (1992) 1929; *Phys. Rev. Lett.* **69** (1992) 458 and *Surf. Sci.* **275** (1992) L682.
- [12] W. Li, G. Vidali and O. Biham, *Phys. Rev. B* **48** (1993) 8336; G. Vidali, O. Biham, H. Zeng, J.-S. Lin and W. Li, in: *The Structure of Surfaces IV*, Eds. S.Y. Tong and X. Xide (World Scientific, Syngapore, 1995).
- [13] H.-J. Ernst, F. Fabre, R. Folkerts and J. Lapujoulade, *Phys. Rev. Lett.* **72** (1994) 112 .
- [14] J.-K. Zuo and J. F. Wendelken, *Phys. Rev. Lett.* **66** (1991) 2227.
- [15] J.-K. Zuo, J.F. Wendelken, H. Durr and C.-L. Liu, *Phys. Rev. Lett.* **72** (1994) 3064.
- [16] H. Durr, J.F. Wendelken and J.-K. Zuo, *Surf. Sci. Lett.* **328** (1995) L527.
- [17] G. L. Kellogg and P. J. Feibelman *Phys. Rev. Lett.* **64** (1990) 3143.
- [18] G. L. Kellogg and A. F. Voter, *Phys. Rev. Lett.* **67** (1991) 622.
- [19] G. L. Kellogg, *Phys. Rev. Lett.* **73** (1994) 1833.
- [20] A. F. Voter, *Phys. Rev.* **B34** (1986) 6819.
- [21] S. Clarke and D. D. Vvedensky, *J. Appl. Phys.* **63** (1988) 2272.
- [22] M.C. Bartelt and J.W. Evans, *Phys. Rev. B* **46** (1992) 12675; M.C. Bartelt, M. C. Tringides and J.W. Evans, *Phys. Rev. B* **47** (1993) 13891.
- [23] M.C. Bartelt and J.W. Evans, *Surf. Sci.* **298** (1993) 421.
- [24] Z. Zhang and H. Metiu, *Surf. Sci. Lett.* **292** (1993) L781.
- [25] G.S. Bales and D.C. Chrzan, *Phys. Rev. B* **50** (1994) 6057.
- [26] C. Ratsch, A. Zangwill, P. Smilauer and D. D. Vvedensky, *Phys. Rev. Lett.* **72** (1994) 3194.
- [27] G. Barkema, O. Biham, M. Breeman, D.O. Boerma and G. Vidali, *Surf. Sci. Lett.* **306** (1994) L569.
- [28] Z. Zhang, X. Chen and M.G. Lagally, *Phys. Rev. Lett.* **73** (1994) 1829.
- [29] M. Schroeder and D.E. Wolf, *Phys. Rev. Lett.* **74** (1995) 2062; D. E. Wolf in *Scale invariance, Interfaces, and Non-Equilibrium Dynamics*, edited by M. Droz, A. J. McKane, J. Vannimenus and D. E. Wolf, Vol. 344 of NATO Advanced Study Institute, Series B: Physics, (Plenum, New York, 1994).
- [30] J. G. Amar, F. Family, *Phys. Rev. Lett.* **74** (1995) 2066.
- [31] C. Ratsch, P. Smilauer, A. Zangwill and D.D Vvedensky, *Surf. Sci.* **329** (1995) L599.
- [32] J. Jacobsen, K.W. Jacobsen, P. Stoltze and J. K. Nørskov, *Phys. Rev. Lett.* **74** (1995) 2295.
- [33] G.S. Bales and D.C. Chrzan, *Phys. Rev. Lett.* **74** (1995) 4879.
- [34] J.G. Amar and F. Family, *Thin Solid Films* **272** (1996) 208; F. Family and J.G. Amar, *Mater. Sci. Eng. B* **30** (1995) 149.
- [35] I. Furman and O. Biham, *Phys. Rev.* **B55** (1997) 7917.
- [36] O. Biham, G.T. Barkema and M. Breeman, *Surf. Sci.* **324** (1995) 47.
- [37] G. Boisvert and L.J. Lewis, *Phys. Rev.* **B56**, (1997) 7643.
- [38] M. Karimi, T. Tomkowski, G. Vidali and O. Biham, *Phys. Rev.* **B52** (1995) 5364.
- [39] M. S. Daw and M. I. Baskes, *Phys. Rev. Lett.* **50** (1983) 1285.
- [40] J. B. Adams, S. M. Foiles, and W. G. Wolfer, *J. Mater. Res.* **4** (1989) 102.
- [41] S. M. Foiles, M. I. Baskes and M. S. Daw, *Phys. Rev.* **B33** (1986) 7983.
- [42] We reduced the neighborhood to a 3×3 square since we found that the three extra sites used in Ref. [27] have little effect.
- [43] Z.-P. Shi, Z. Zhang, A.K. Swan and J.F. Wendelken, *Phys. Rev. Lett.* **76** (1996) 4927.
- [44] M. Breeman, G.T. Barkema and D.O. Boerma, *Surf. Sci.* **303** (1994) 25.

Table Captions

- [45] M.W. Finnis and J.E. Sinclair, *Phil. Mag.* **A50** (1984) 45.
- [46] In experiments, no significant nucleation was observed on top of islands up to nearly full coverage [6,11]. Therefore, in our simulations an atom deposited on top of an island hops randomly until it jumps down to the lower layer.
- [47] K. Fichtorn and W. H. Weinberg, *J. Chem. Phys.* **95** (1991) 1090.
- [48] Y.-T Lu and H. Metiu, *Surf. Sci.* **245** (1991) 150.
- [49] S. Clarke, M.R. Wilby and D.D. Vvedensky, *Surf. Sci.* **255** (1991) 91.
- [50] H. C. Kang and W. H. Weinberg, *Surf. Sci.* **299** (1994) 755.
- [51] S. Stoyanov and D. Kashchiev, *Current Topics in Material Science* **7** (1981) 70.
- [52] J. A. Venables, G. D. T. Spiller, and M. Hanbucken, *Rep. Prog. Phys.* **47** (1984) 399 .
- [53] L. Tang, *J. Phys. I France* **3** (1993) 935.
- [54] M.C. Bartelt, L.S. Perkins and J.W. Evans, *Surf. Sci. Lett.* **344** (1995) L1193.
- [55] J. Villain, A. Pimpinelli, and D. Wolf, *Comments Cond. matt. Phys.* **16** (1992) 1; J. Villain, A. Pimpinelli, L. Tang, and D. Wolf, *J. Phys. I France* **2** (1992) 2107.
- [56] J.-M. Wen, J.W. Evans, M.C. Bartelt, J.W. Burnett and P.A. Thiel, *Phys. Rev. Lett.* **76** (1996) 652.
- [57] To demonstrate that our models are applicable to Ni(001) and Ag(001) we present here the results of EAM calculations for the six configurations in the first row of Table I. For Ni(001) these barriers are $E_B^n = 0.06, 0.35, 0.25, 0.62, 0.63$ and 1.02 eV for $n = 68, 76, 4, 12, 0$ and 8 respectively. For Ag(001) these barriers are $E_B^n = 0.14, 0.35, 0.21, 0.46, 0.47$ and 0.71 eV for $n = 68, 76, 4, 12, 0$ and 8 respectively. We observe that in both cases barriers which belong to different peaks are typically separated by 0.2eV or more.
- [58] P. J. Feibelman *Phys. Rev. Lett.* **65** (1990) 729.
- [59] C.L. Liu, J.M. Cohen, J.B. Adams and A.F. Voter, *Surf. Sci.* **253** (1991) 334.
- [60] R. Stumpf and M. Scheffler, *Phys. Rev. Lett.* **72** (1994) 254.
- [61] R. Stumpf and M. Scheffler, *Phys. Rev.* **B53** (1996) 4958.

TABLE I. The hopping energy barriers obtained from the EAM calculations for all 128 possible configurations within a 3×3 square around the hopping atom. The barriers are given in eV. Each number in the Table is the barrier E_B^n for the configuration in which the occupied sites are the union of the occupied sites in the picture on top of the given column (indexed by n_1) and on the left hand side of the given row (indexed by n_2). Consequently, the index n specifying the barrier is given by $n = n_1 + n_2$.

TABLE II. Diffusion coefficients of small islands of sizes $s = 1, 2, 3, 5, 7$ atoms as measured from MC simulations of single islands. Results are shown for the EAM, model I and model II barriers at $T = 250\text{K}$. Islands of sizes $s = 4, 6$ and $s \geq 8$ were found to be immobile at this temperature.

Table I

		Peak I	Peak II	Peak III	Peak IV		
$n_1 \rightarrow$		68	76	12	0	8	
$n_2 \downarrow$							
0		0.01	0.25	0.18	0.48	0.48	0.81
1		0.02	0.28	0.25	0.53	0.46	0.85
2		0.02	0.21	0.18	0.44 (0.34)	0.46	0.74 (0.60)
3		0.05	0.25	0.24	0.48	0.54	0.78 (0.65)
16		0.02	0.28	0.21	0.50	0.46	0.85
17		0.04	0.30	0.28	0.54	0.66	0.89
18		0.05	0.27	0.23	0.49	0.52	0.80
19		0.08	0.29	0.29	0.52	0.61	0.83
32		0.02	0.21	0.18	0.48	0.46	0.74 (0.60)
33		0.05	0.27	0.28	0.54	0.52	0.80
34		0.05	0.24	0.28	0.50 (0.16)	0.55	0.78 (0.37)
35		0.08	0.26 (0.08)	0.33	0.49	0.62	0.81 (0.47)
48		0.05	0.25	0.28	0.51	0.54	0.78 (0.65)
49		0.08	0.29	0.33	0.56	0.61	0.83

							
50		0.08	0.26 (0.08)	0.34	0.51 (0.22)	0.62	0.81 (0.47)
51		0.13	0.28 (0.12)	0.40	0.53 (0.36)	0.70	0.69

Table II

Cluster Size	Diffusion Coefficients [hops/s]		
	EAM	model 1	model 2
1	172 ± 5	118 ± 4	24.3 ± 0.8
2	237 ± 8	55 ± 2	13.2 ± 0.4
3	5.6 ± 0.2	12.4 ± 0.4	5.9 ± 0.2
5	1.12 ± 0.04	0.94 ± 0.03	1.00 ± 0.03
7	0.28 ± 0.02	0.34 ± 0.01	0.42 ± 0.02

Figure Captions

Fig. 1: Classification of all possible local environments of a hopping atom including seven adjacent sites. Each site can be either occupied or unoccupied, giving rise to $2^7 = 128$ local environments. Sites 1, 3 and 5 are nearest neighbors of the original site while sites 1, 2, 5 and 6 are adjacent to the bridge site that the atom has to pass.

Fig. 2: The distribution of hopping energy barriers obtained from EAM calculations (a) and from model I (b) for the 128 possible local environments of Fig. 1. According to model I the lowest and highest peaks include 16 barriers each, while the middle peaks include 48 barriers each. The EAM peaks are broad and some overlap occurs.

Fig. 3: Snapshots of surface morphologies obtained in MC simulations using the EAM (a), model I (b), and model II (c) barriers. The simulations were carried out on a 250×250 lattice at $T = 250\text{K}$ and deposition rate $F = 0.01$ ML/s. The snapshots presented are at coverage $\theta = 0.1$ ML. In all three cases the islands form generally compact square and rectangular shapes with a small number of kinks.

Fig. 4: The island density vs. coverage is presented for the EAM (*), model I (o) and model II (+) barriers. In all cases the island density quickly increases at low coverage. It then saturates and remains nearly constant within the quasi-steady state aggregation dominated regime. The solid line is a guide to the eye.

Fig. 5: Snapshots of the island morphology obtained from MC simulations using the EAM barriers for three deposition rates: (a) 0.1; (b) 0.01 and (c) 0.001 ML/s. The simulations were done on a 250×250 lattice at $T = 250\text{K}$ and the snapshots were taken at $\theta = 0.1$ ML. It is observed that decreasing the deposition rate gives rise to fewer and larger islands.

Fig. 6: The island density vs. coverage is presented for the EAM barriers, at deposition rates (from top to bottom) $F = 0.1, 0.04, 0.01, 0.004, 0.001$ and 0.0004 ML/s. The island density decreases as the deposition rate is lowered. Also, the plateau associated with the aggregation dominated regime broadens. The solid line is a guide to the eye.

Fig. 7: The island density vs. deposition rate for the EAM (*), model I (o) and model II (+) barriers. These results were obtained at $T = 250\text{K}$ and $\theta = 0.1$ ML for deposition rates between $F = 0.1$ and 0.0004 ML/s. The best fit through the six data points in each of the three models gives $\gamma = 0.32 \pm 0.01$ for the EAM, 0.33 ± 0.01 for model I and 0.31 ± 0.01 for model II barriers. These results indicate that models I and II provide a good description of the scaling properties.

Fig. 8: Scaled island size distributions are shown for the EAM (a), model I (b), and model II (c) barriers. \bar{s} is the average island size. The deposition rates examined in each case are $F = 10^{-1}$ (*), 10^{-2} (o) and 10^{-3} ML/s (+). These results are based on 20 runs on a 250×250 size lattice at $T = 250\text{K}$ and $\theta = 0.1$ ML.

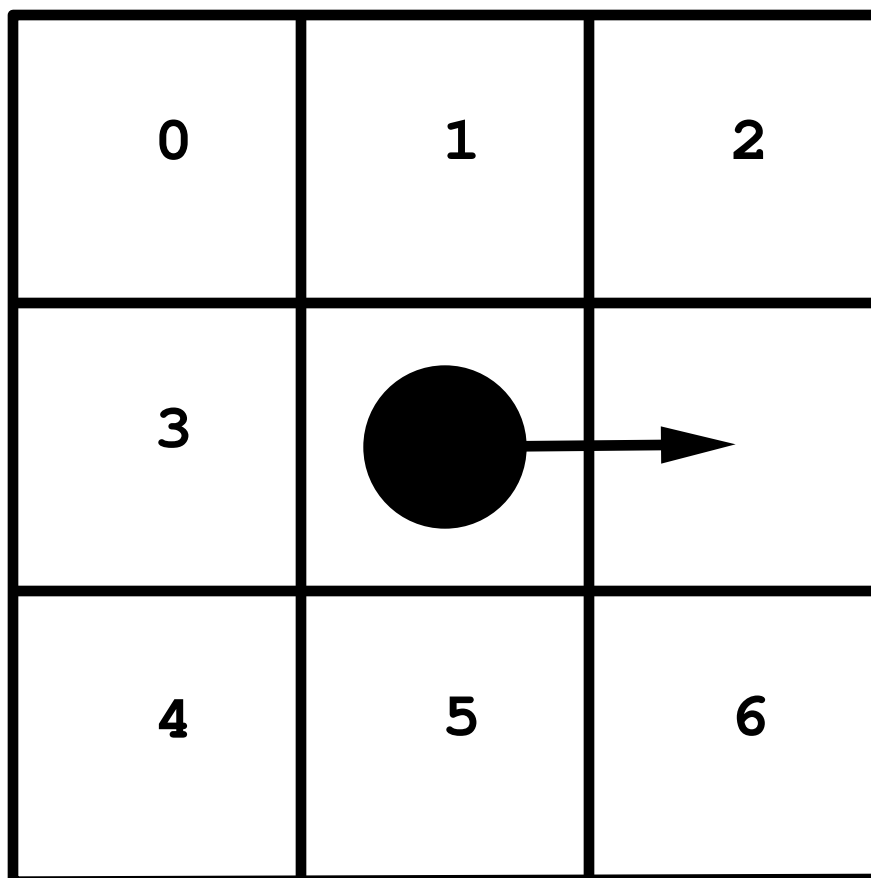


Fig. 1

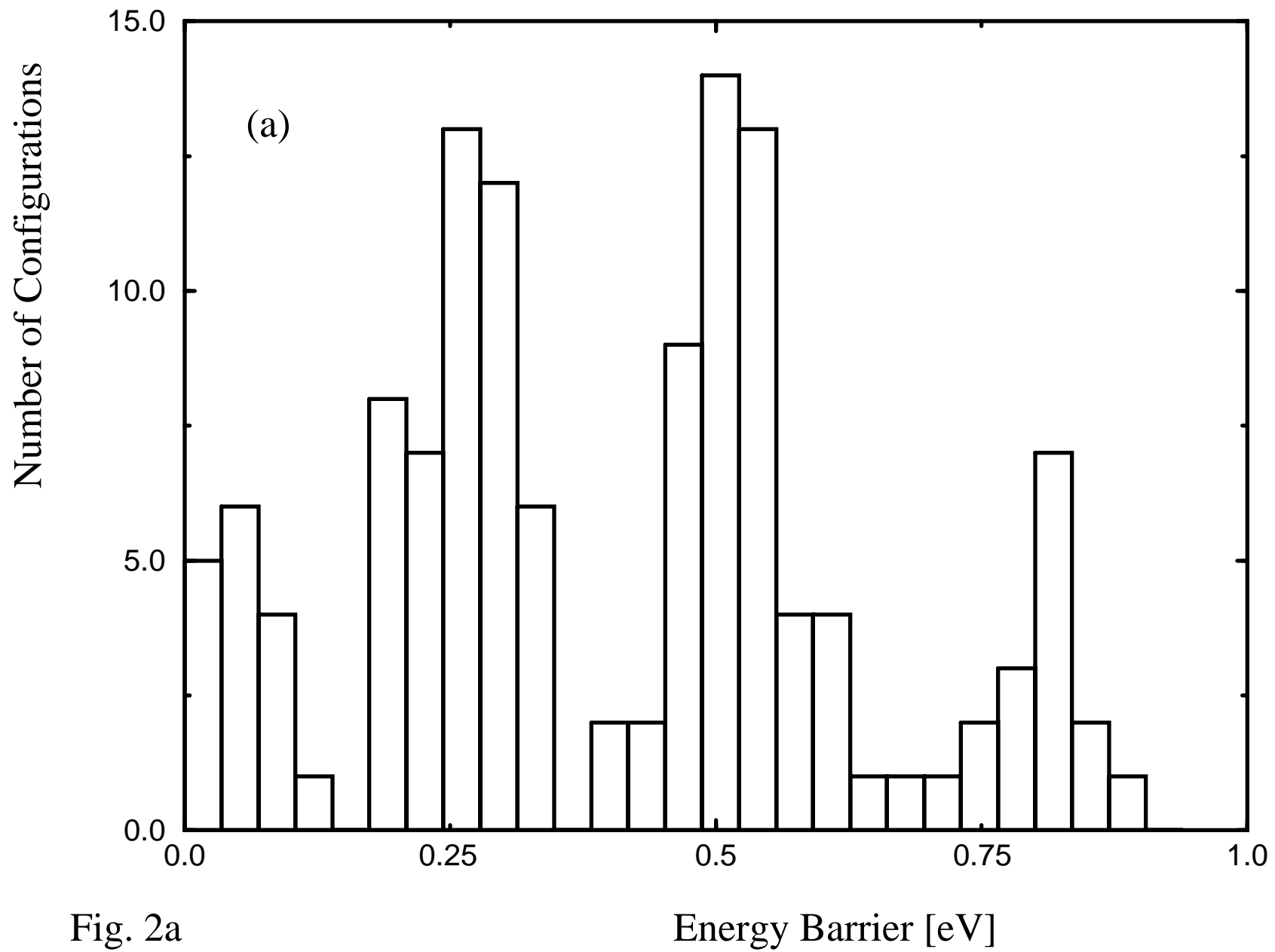


Fig. 2a

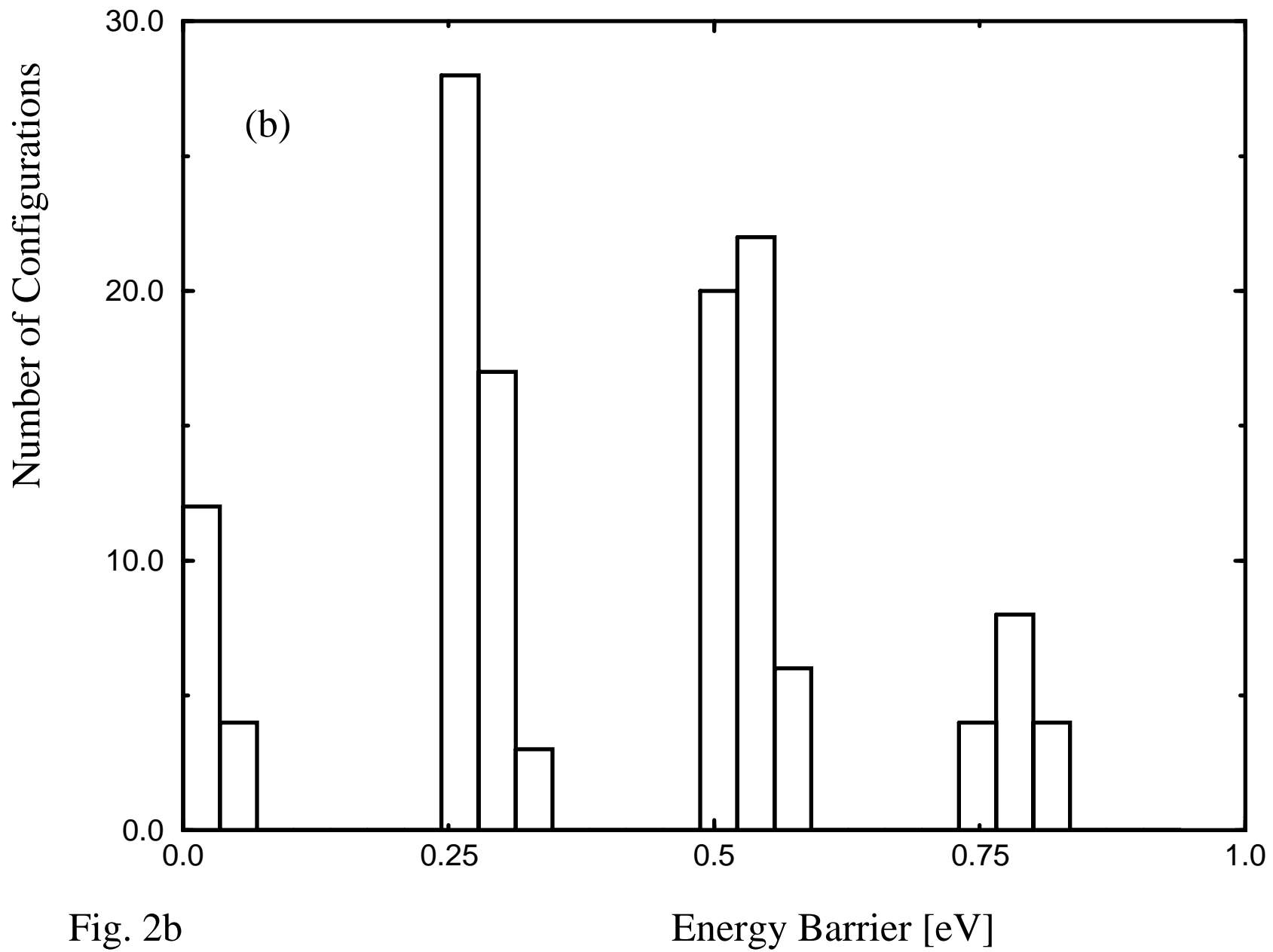


Fig. 2b

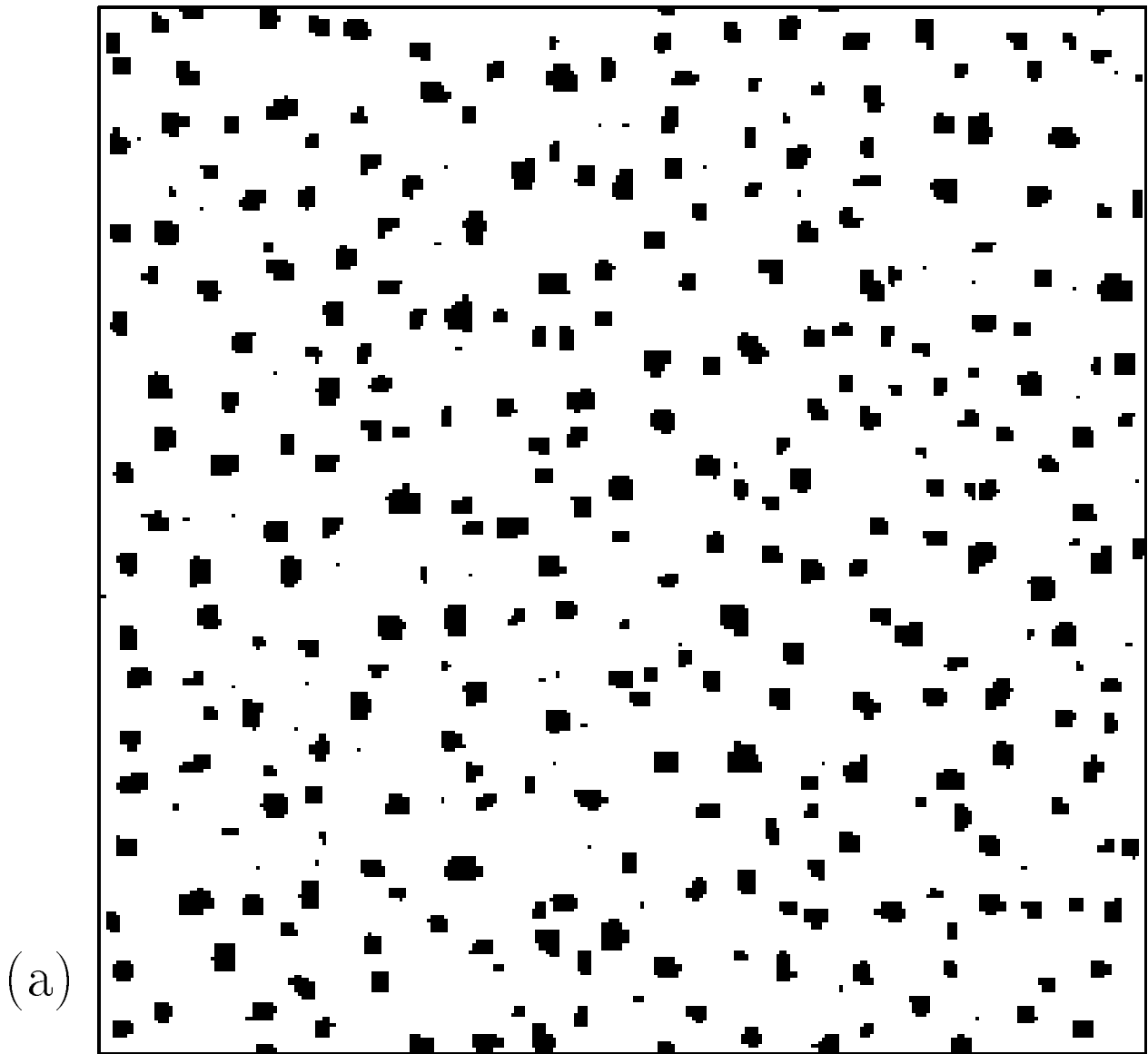


FIG. 3a

(b)

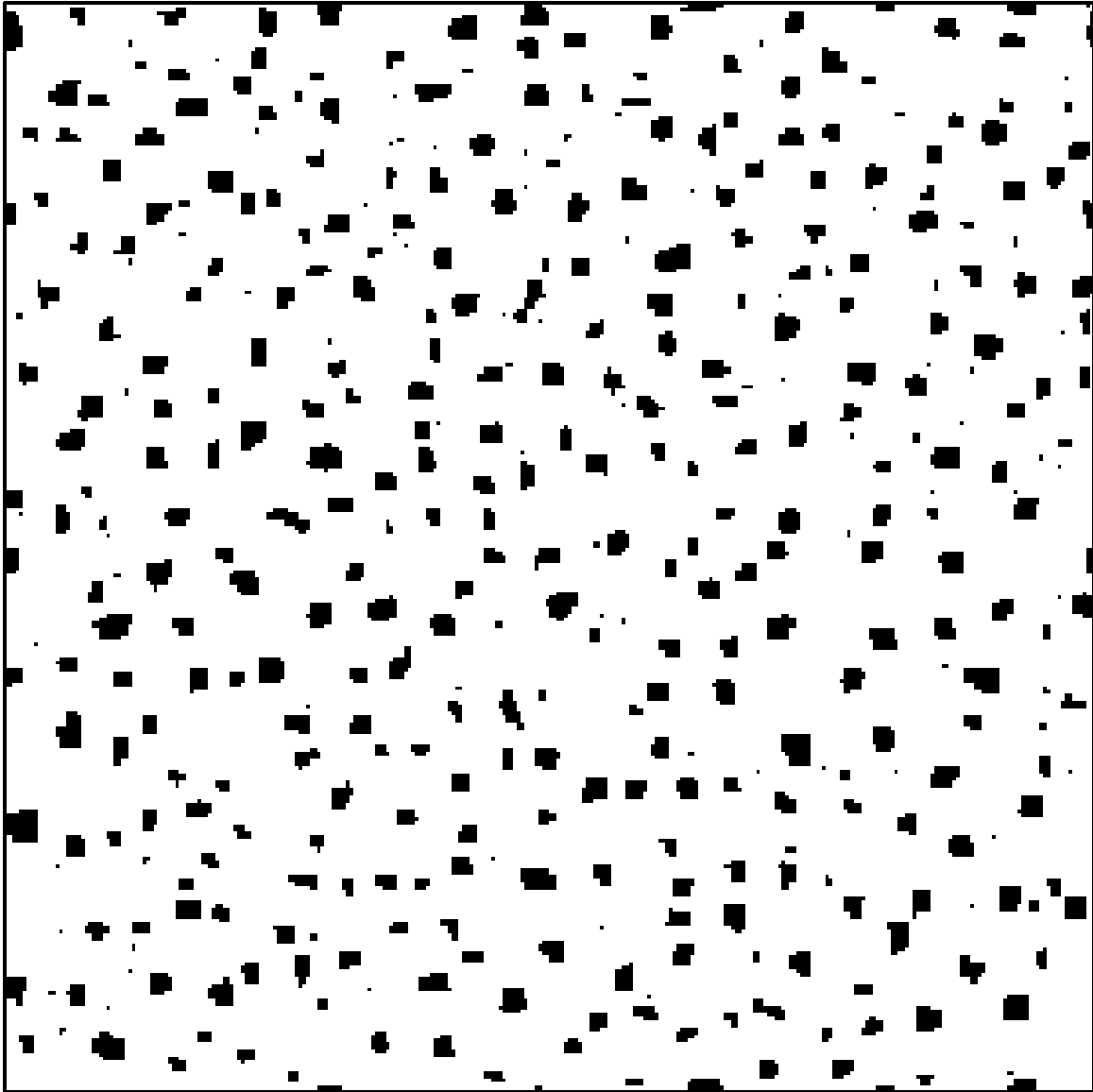


FIG. 3b

(c)

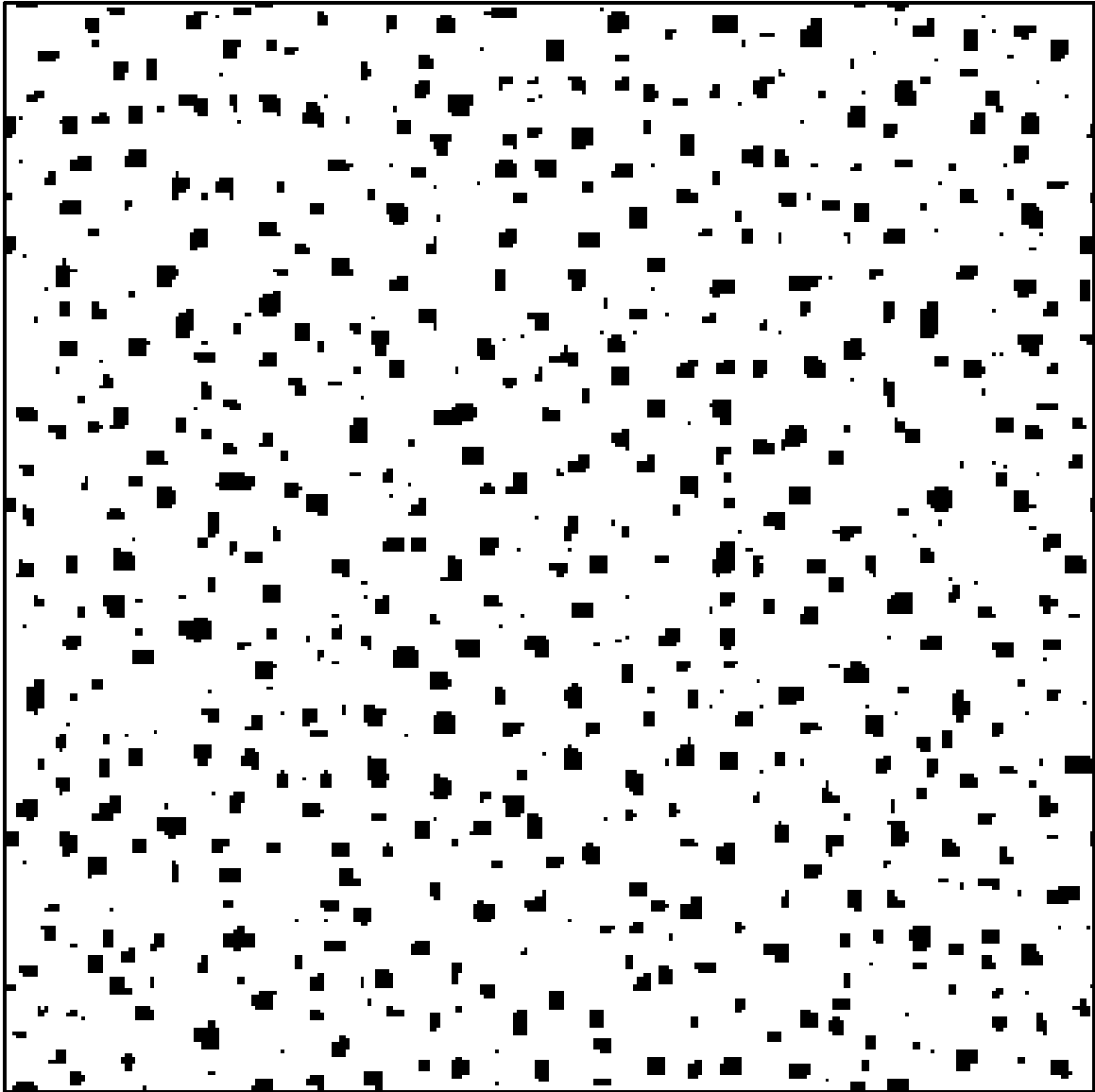


FIG. 3c

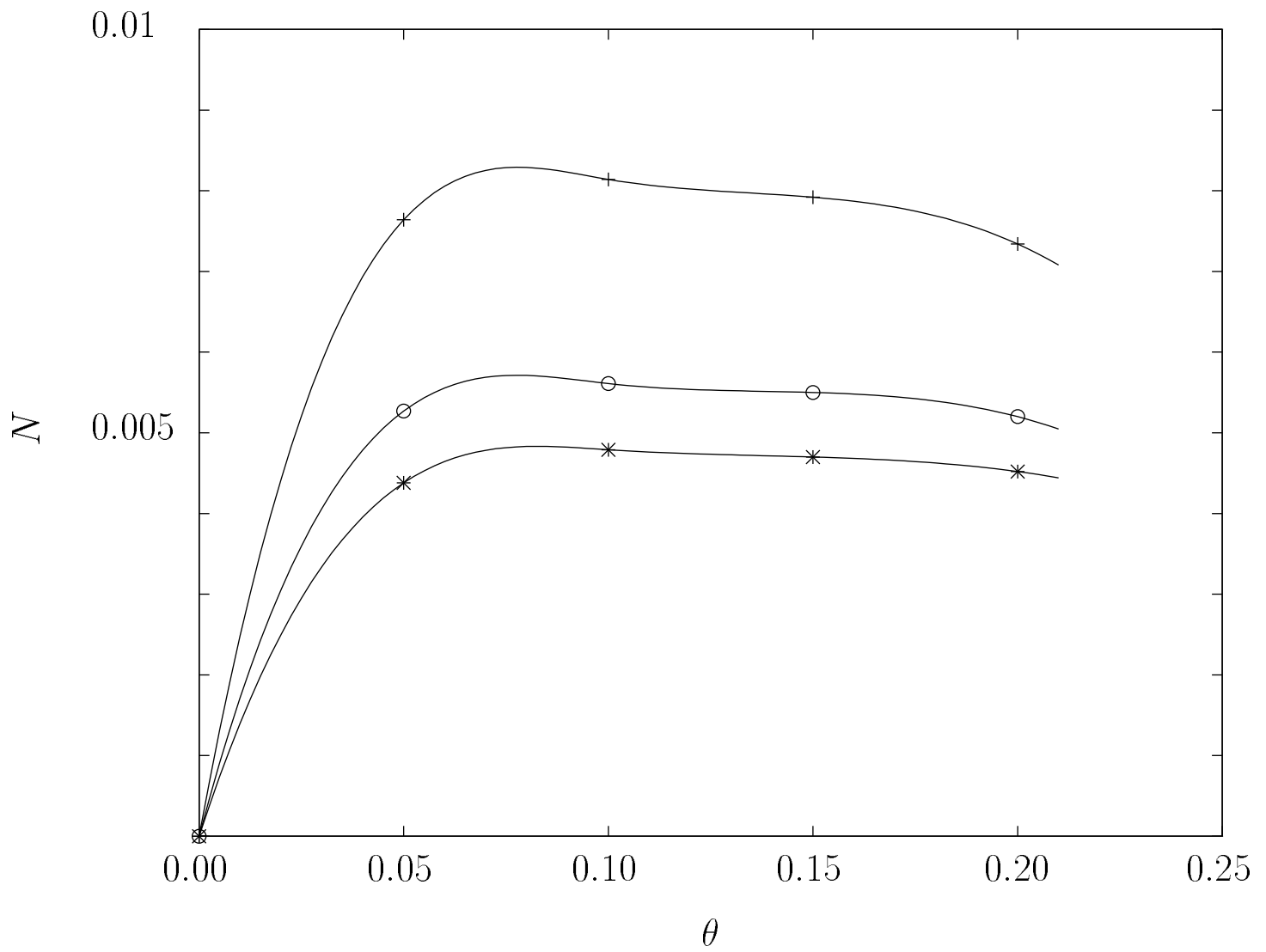


FIG. 4

(a)

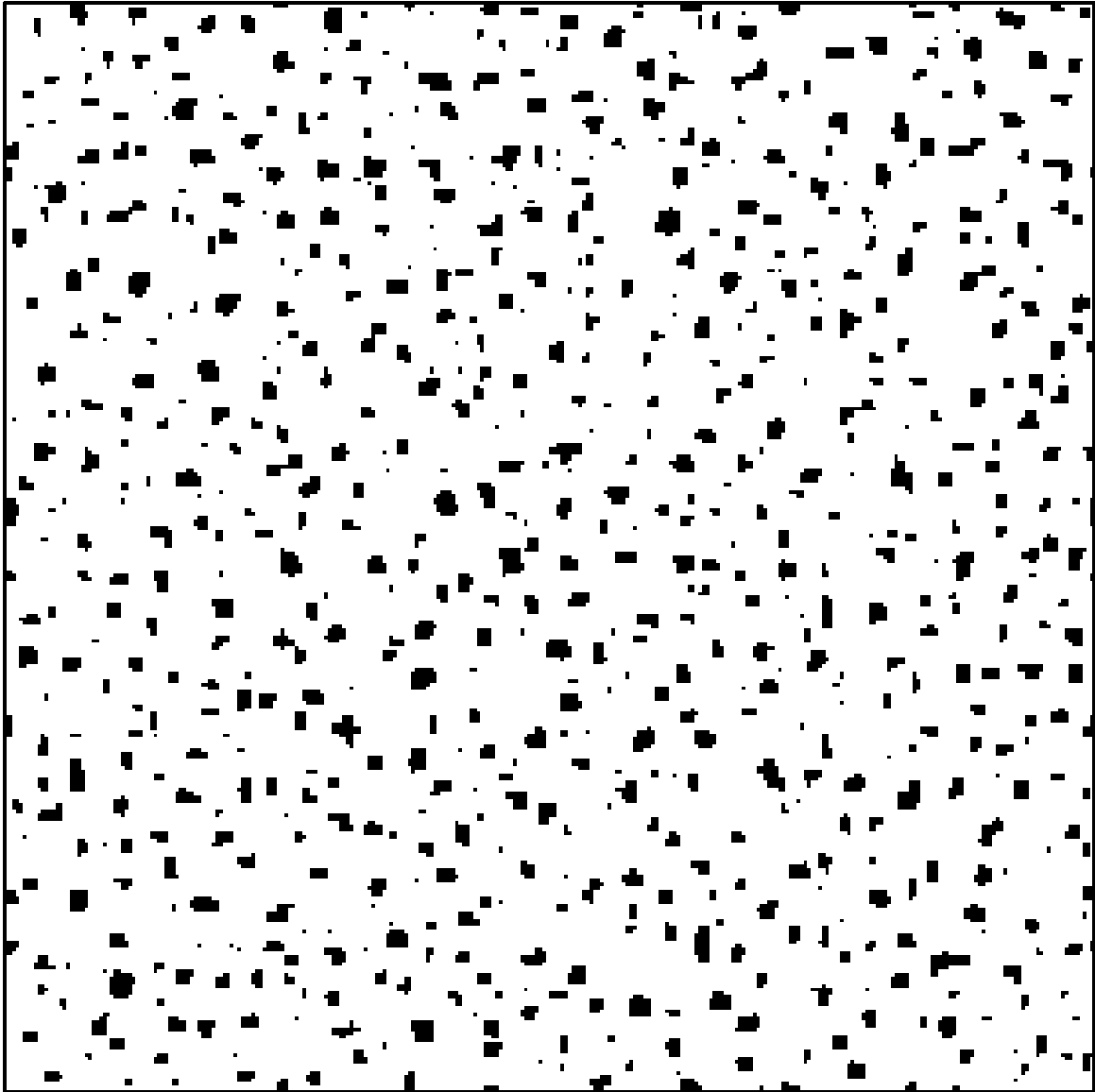


FIG. 5a

(b)

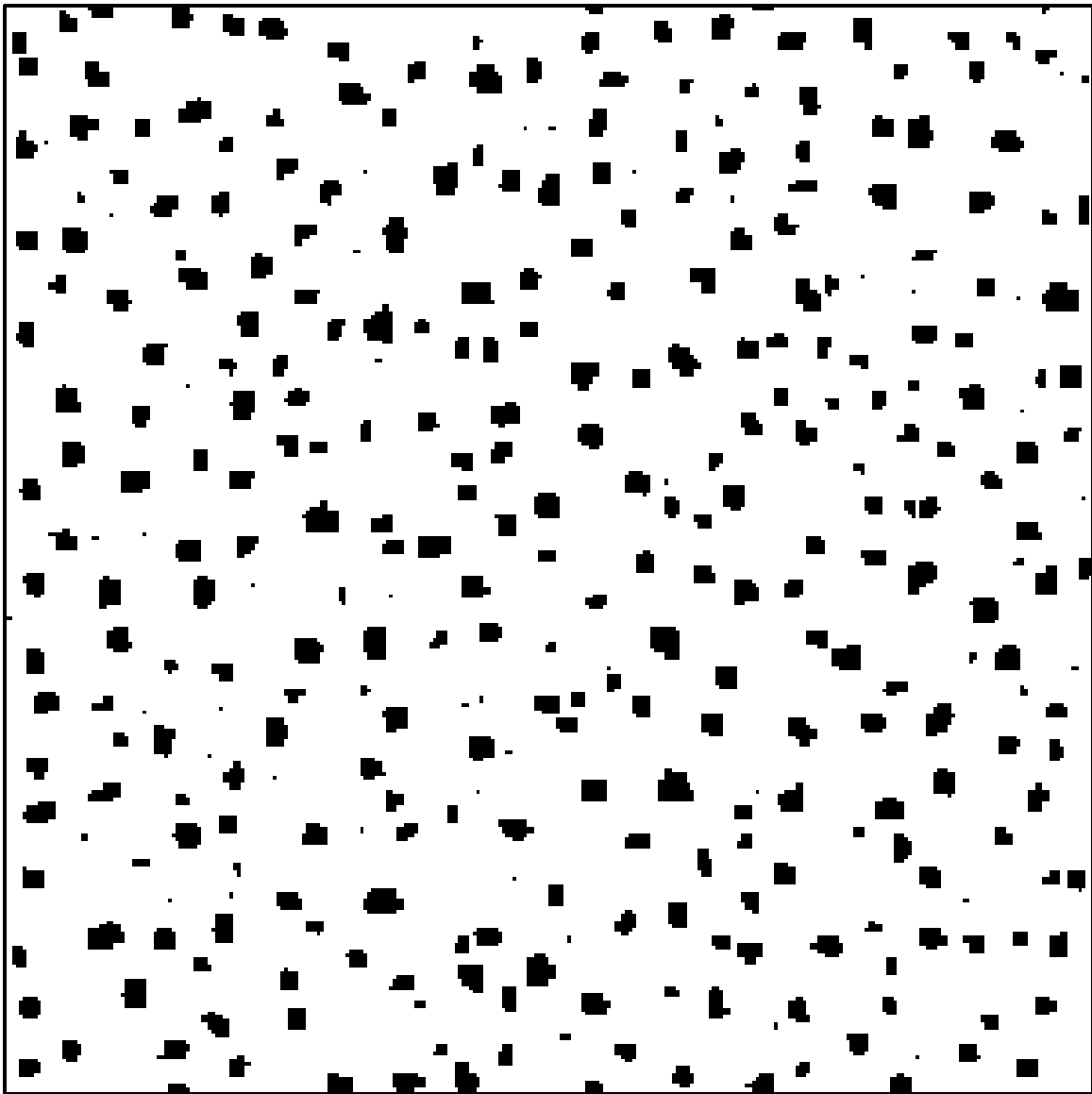


FIG. 5b

(c)

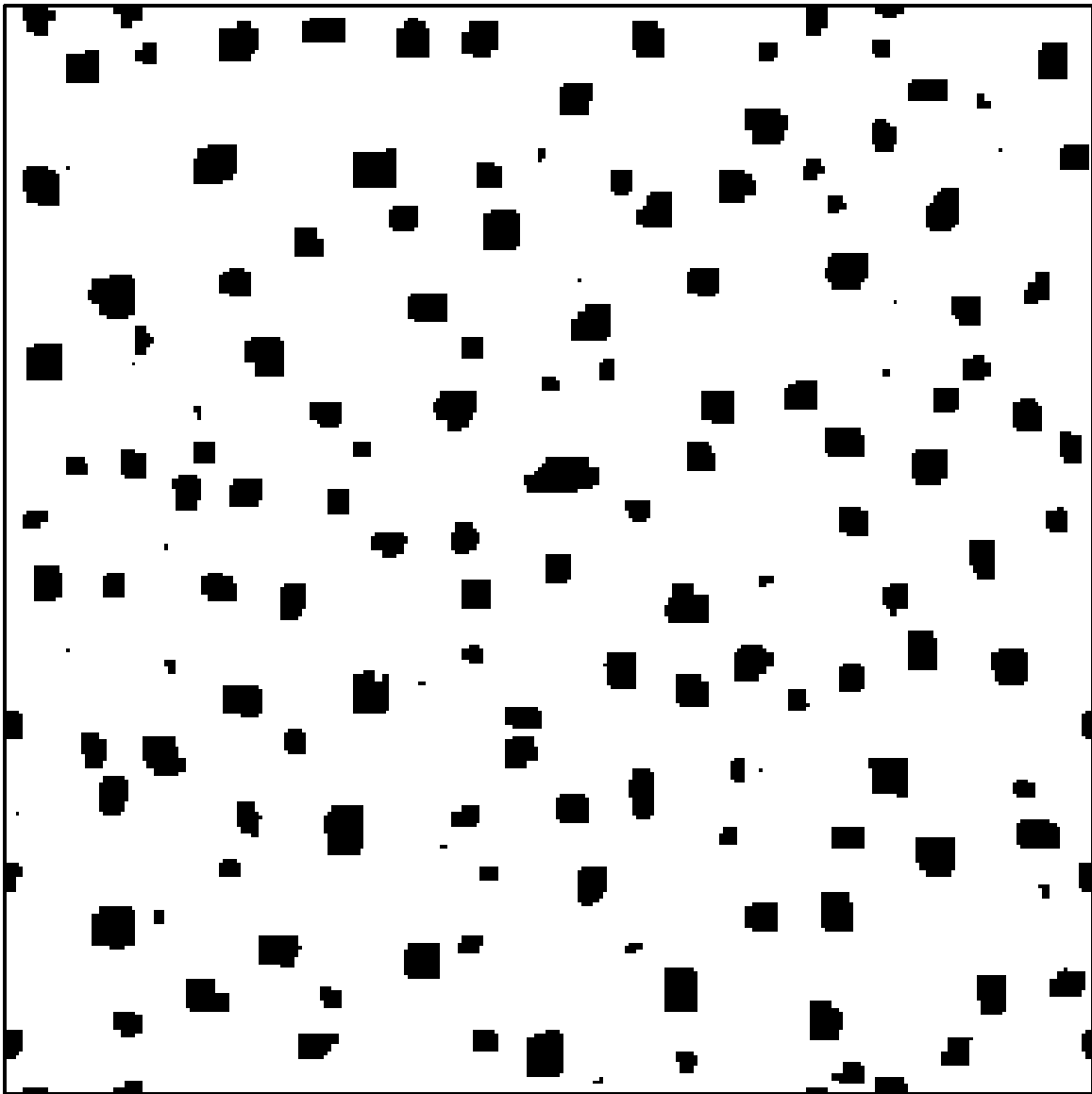


FIG. 5c

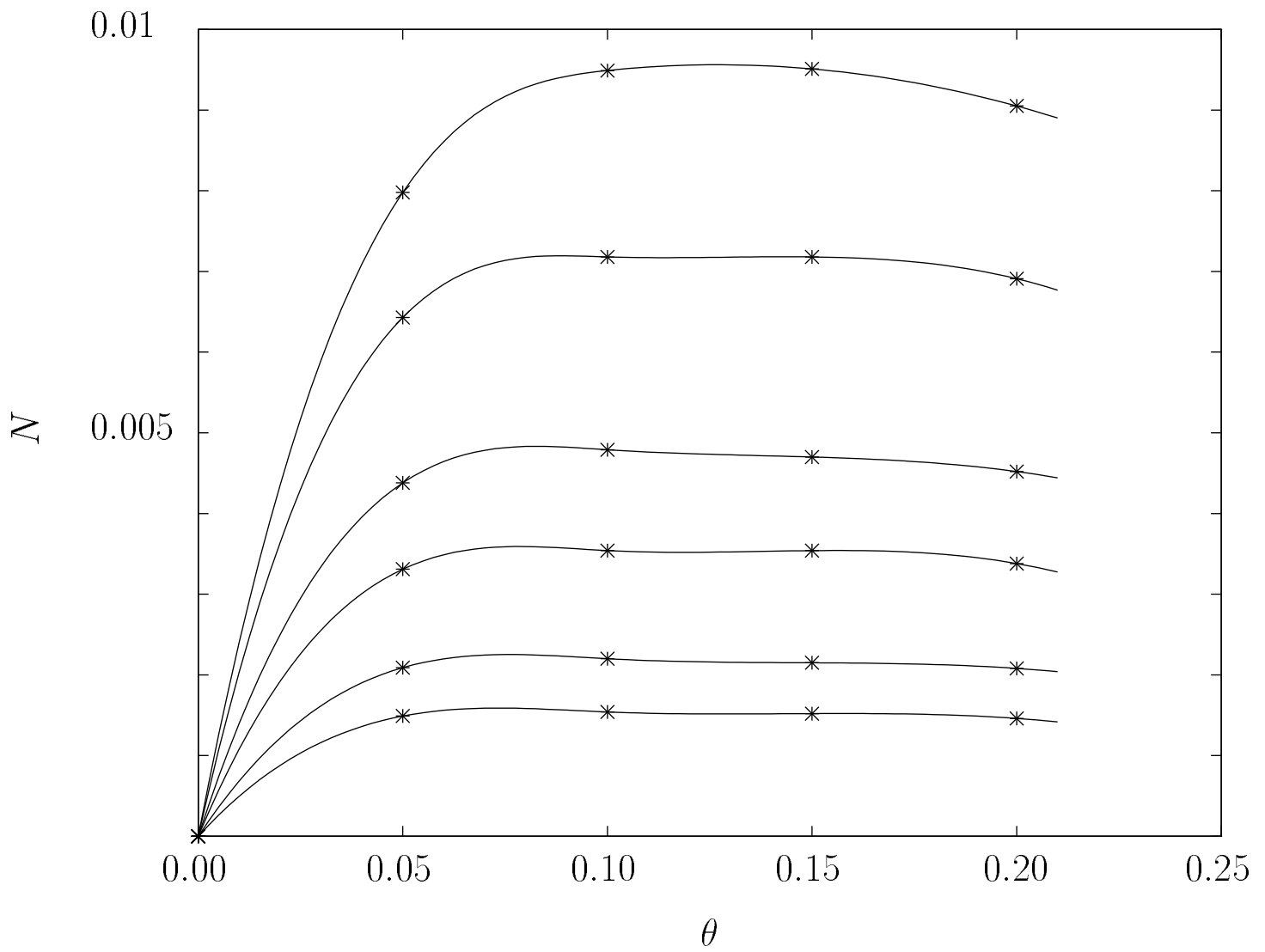


FIG. 6

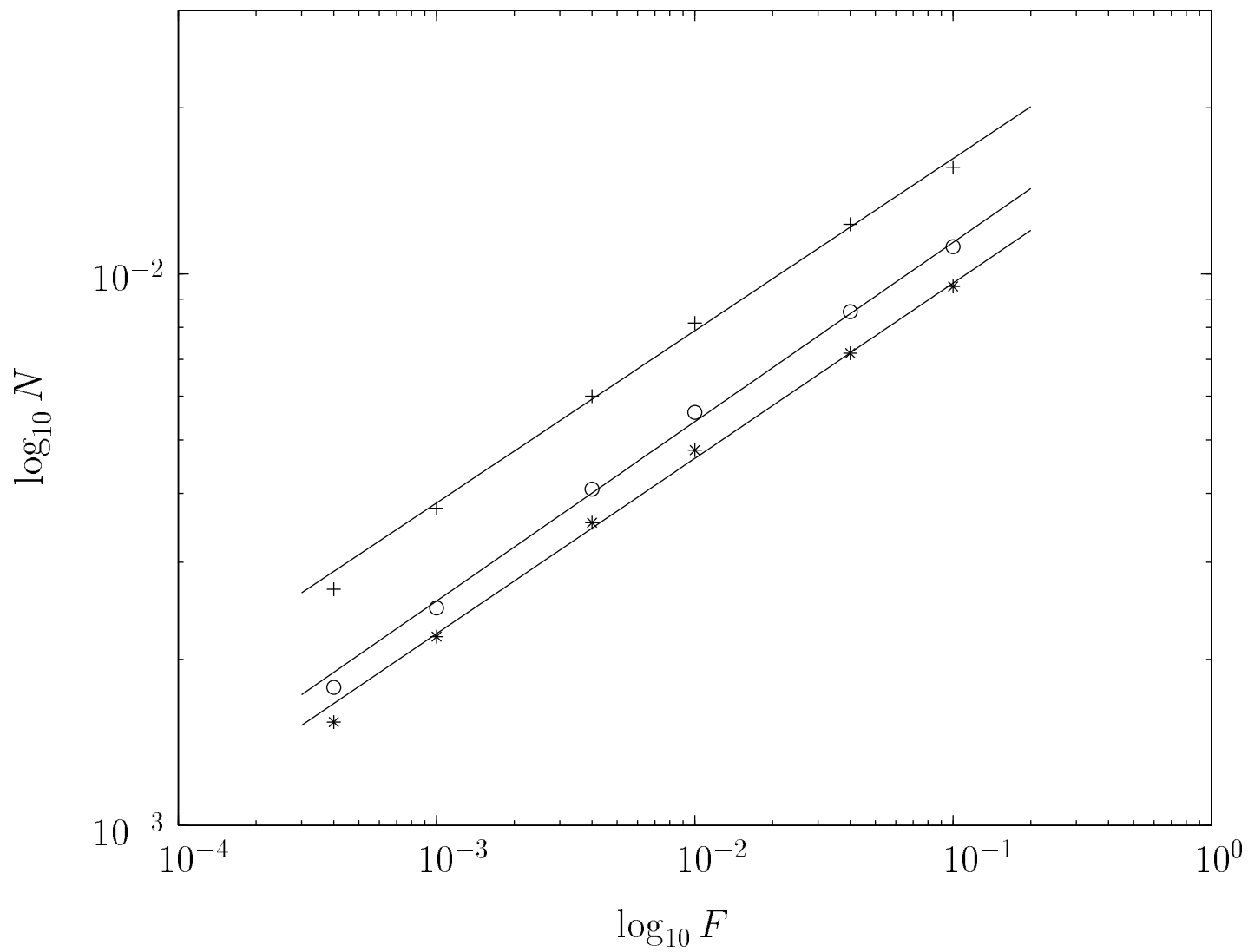


FIG. 7

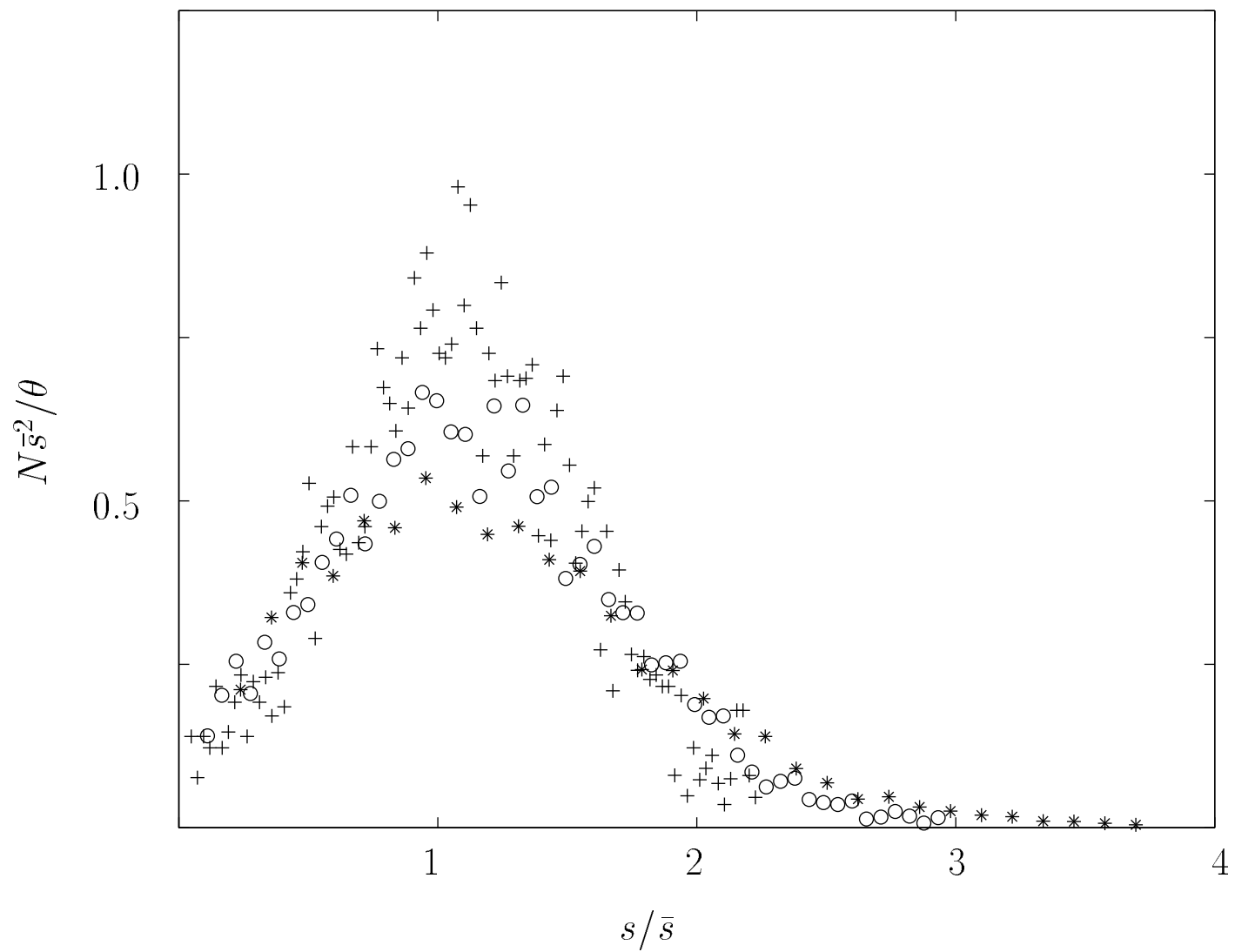


FIG. 8a

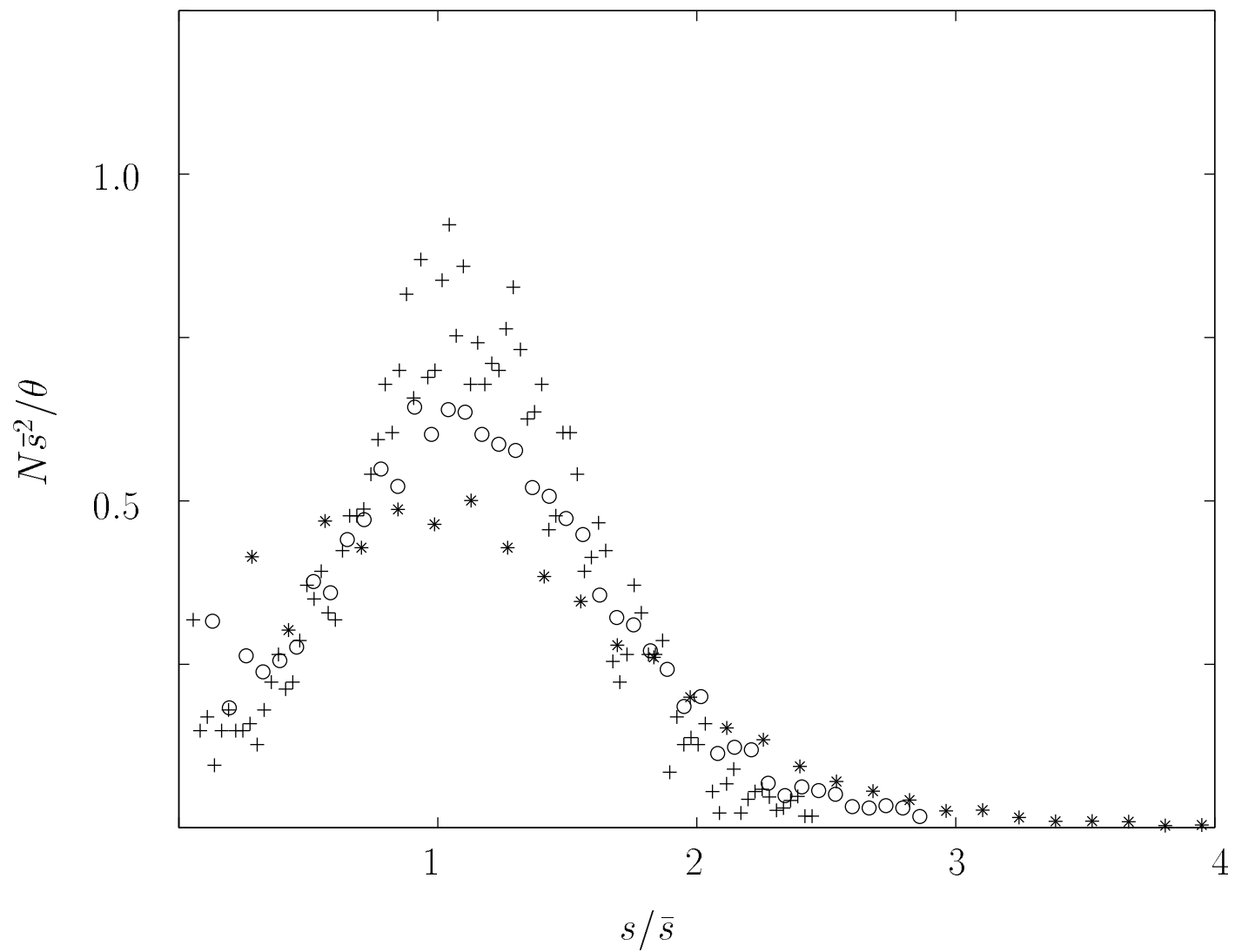


FIG. 8b

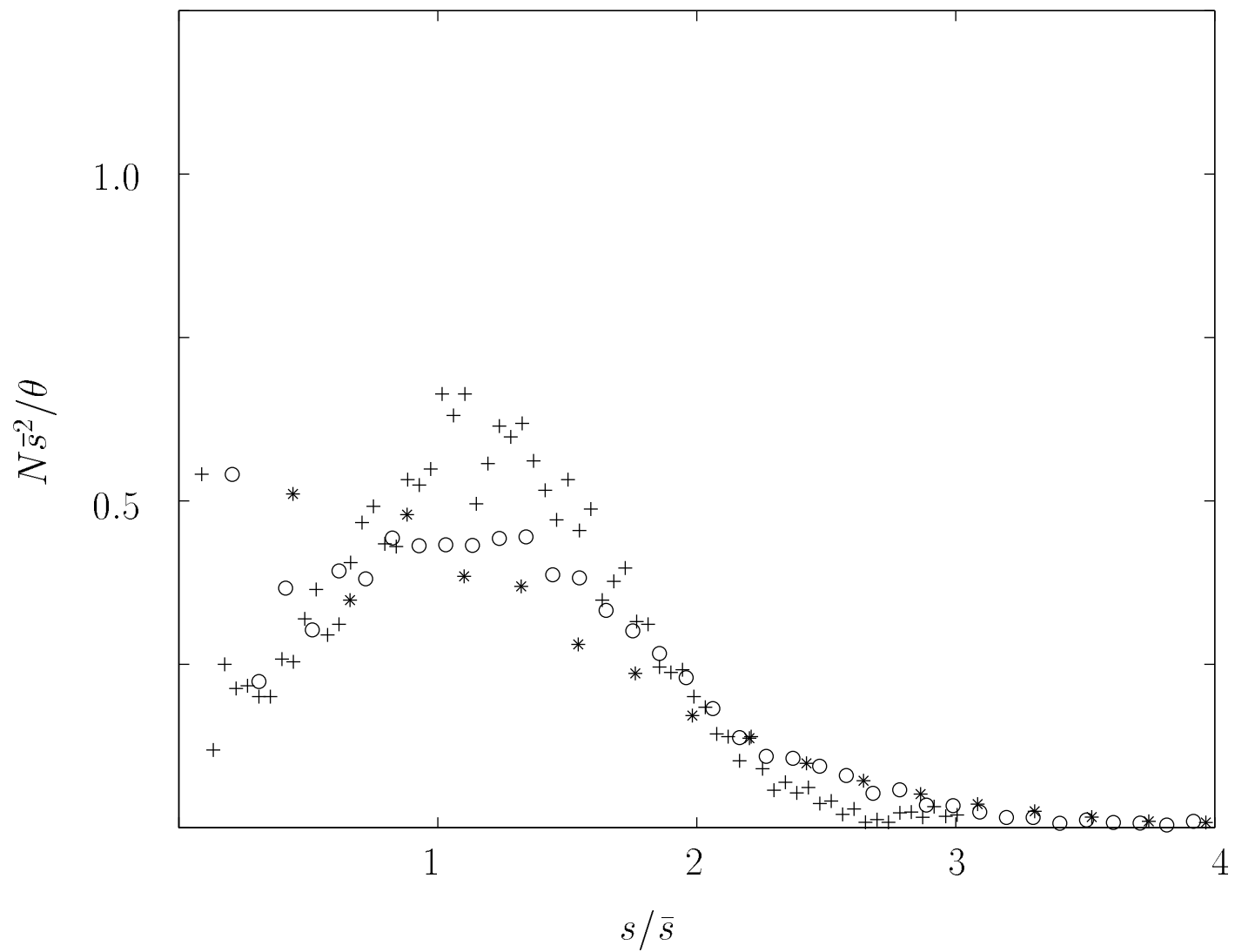


FIG. 8c